

# *The role of the timing of Sudden Stratospheric Warmings for precipitation and temperature anomalies in Europe*

Article

Published Version

Creative Commons: Attribution 4.0 (CC-BY)

Open Access

Monnin, E., Kretschmer, M. ORCID: <https://orcid.org/0000-0002-2756-9526> and Polichtchouk, I. (2021) The role of the timing of Sudden Stratospheric Warmings for precipitation and temperature anomalies in Europe. International Journal of Climatology. ISSN 0899-8418 doi: <https://doi.org/10.1002/joc.7426> Available at <https://centaur.reading.ac.uk/101090/>

It is advisable to refer to the publisher's version if you intend to cite from the work. See [Guidance on citing](#).

To link to this article DOI: <http://dx.doi.org/10.1002/joc.7426>

Publisher: John Wiley & Sons

All outputs in CentAUR are protected by Intellectual Property Rights law, including copyright law. Copyright and IPR is retained by the creators or other copyright holders. Terms and conditions for use of this material are defined in the [End User Agreement](#).

[www.reading.ac.uk/centaur](http://www.reading.ac.uk/centaur)

**CentAUR**

Central Archive at the University of Reading

Reading's research outputs online

RESEARCH ARTICLE

# The role of the timing of sudden stratospheric warmings for precipitation and temperature anomalies in Europe

Erika Monnin<sup>1</sup> | Marlene Kretschmer<sup>2</sup>   | Inna Polichtchouk<sup>3</sup> 

<sup>1</sup>ENSTA Paris, Palaiseau, France

<sup>2</sup>Department of Meteorology, University of Reading, Reading, UK

<sup>3</sup>European Centre for Medium-Range Weather Forecasts, Reading, UK

## Correspondence

Marlene Kretschmer, Department of Meteorology, University of Reading, Reading, UK.  
Email: m.j.a.kretschmer@reading.ac.uk

## Funding information

Marlene Kretschmer has received funding from the European Union's Horizon 2020 research and innovation programme under the Marie Skłodowska-Curie grant agreement (No. 841902).

## Abstract

The Northern Hemisphere stratospheric polar vortex (SPV), a band of fast westerly winds over the Pole extending from approximately 10 to 50 km altitude, is a key driver of European winter weather. Extremely weak polar vortex states, so called sudden stratospheric warmings (SSWs), are on average followed by dry and cold weather in Northern Europe, as well as wetter weather in Southern Europe. However, the surface response of SSWs varies greatly between events, and it is not well understood which factors modulate this difference. Here, we address the role of the timing of SSWs within the cold season (December–March) for the temperature and precipitation response in Europe. Given the limited sample size of SSWs in the observations, hindcasts of the seasonal forecasting model SEAS5 from the European Centre for Medium-Range Weather Forecasts are analysed. First, we evaluate key characteristics of stratosphere–troposphere coupling in SEAS5 against reanalysis data and find them to be reasonably well captured by the model, justifying our approach. We then show that in SEAS5, early winter (December and January) SSWs are followed by more pronounced surface impacts compared to late winter (February and March) SSWs. For example, in Scotland, the low precipitation anomalies are roughly twice as severe after early winter SSWs than after late winter SSWs. The difference in the response cannot be explained by more downward propagating SSWs in early winter, or by different monthly precipitation climatologies. Instead, we demonstrate that the differences result from stronger SPV anomalies associated with early winter SSWs. This is a statistical artefact introduced through the commonly used SSW event definition, which involves an absolute threshold, and, therefore, leads to stronger SPV anomalies during early winter SSWs when the stratospheric mean state is stronger. Our study highlights the sensitivity of surface impacts to SSW event definition.

## 1 | INTRODUCTION

A key driver of European weather and climate is the Northern Hemisphere stratospheric polar vortex (SPV) (Baldwin and Dunkerton, 2001; Kretschmer *et al.*, 2018a,

2018b; King *et al.*, 2019; Domeisen and Butler, 2020). The SPV is a band of strong westerly winds in the Arctic stratosphere that forms during boreal autumn (Vaughan *et al.*, 2017). It stems from a strong temperature gradient between the Arctic and the lower latitudes due to the

This is an open access article under the terms of the Creative Commons Attribution License, which permits use, distribution and reproduction in any medium, provided the original work is properly cited.

© 2021 The Authors. *International Journal of Climatology* published by John Wiley & Sons Ltd on behalf of Royal Meteorological Society.

lack of incoming solar radiation over the Arctic during the cold season, and it disappears again in spring when sunlight returns to the Pole.

Extreme weak phases of the SPV, such as major sudden stratospheric warmings (SSWs), during which the vortex breaks down and the winds in the stratosphere reverse, can affect the tropospheric circulation below (Baldwin and Dunkerton, 2001; Waugh *et al.*, 2017). In particular, SSWs are often followed by a persistent negative phase of the North Atlantic Oscillation (NAO) and the associated weather patterns. For instance, in the weeks after SSWs, there is usually increased precipitation over Southern Europe while Northern Europe experiences more cold and dry weather conditions (Beerli and Grams, 2019; King *et al.*, 2019). In addition to its importance for subseasonal and seasonal surface variability, the SPV is also a driver of surface conditions on decadal time scales (Kidston *et al.*, 2015). In what way the SPV will change under global warming was further demonstrated to largely determine future changes in European precipitation and extreme windiness (Karpechko and Manzini, 2012; Scaife *et al.*, 2012; Zappa and Shepherd, 2017).

While the observed average effects of SSWs for Europe are well documented (Ayarzagüena *et al.*, 2018; Kretschmer *et al.*, 2018a; King *et al.*, 2019; Afargan-Gerstman and Domeisen, 2020; Kautz *et al.*, 2020), the surface impacts vary strongly across events. Only roughly half of the observed SSWs have been classified as downward propagating events, meaning that the stratospheric anomalies were followed by the canonical NAO response in the troposphere (Karpechko *et al.*, 2017). For the other events, so-called non-downward propagating SSWs, the stratospheric circulation anomalies were mostly confined to the stratosphere. As the exact downward coupling mechanisms of SSWs are not understood (e.g., Hitchcock and Simpson, 2014), it is also not clear which factors modulate this difference.

To better understand the variability in the surface response of SSWs, several previous studies classified SSWs according to different event characteristics. For example, SSWs have been distinguished by their horizontal spatial structure (vortex split vs. vortex displacement events), although no strong differences in the tropospheric circulation response were found when analysing a large set of events in a climate model (Maycock and Hitchcock, 2015). Moreover, differences in the troposphere–stratosphere coupling mechanism have been addressed (absorptive vs. reflective events), with the absorbing-type events, in particular, being associated with downward propagating SSWs and the canonical NAO surface response (Kodera *et al.*, 2016; Kretschmer *et al.*, 2018a; Matthias and Kretschmer, 2020). Recent

studies also tackled the importance of the prevailing North Atlantic weather regime during the occurrence of SSWs and addressed how this modulates the surface response (Beerli and Grams, 2019; Domeisen *et al.*, 2020). For example, Domeisen *et al.* (2020) found that high pressure anomalies over Greenland (which project onto the negative phase of the NAO) are more likely to happen when the regime during the SSW onset is a European Blocking regime (negative pressure anomalies over western Europe). Overall, several factors likely contribute to the surface response, but which and how exactly remains an open question.

The purpose of this study is to investigate whether the *timing* of a SSW within the cold season (from December to March) plays a role in the surface response. Such differences have been documented for other drivers of European weather and climate, such as the El Niño Southern Oscillation (Jiménez-Estève and Domeisen, 2018; King *et al.*, 2021), but have as of yet not been documented for SSWs. While SSWs are linked to a range of extreme events in different regions (Domeisen and Butler, 2020), here, we focus on anomalous temperature and precipitation in Europe.

Due to the limited observational record, we make use of the large-ensemble hindcasts SEAS5 of the seasonal prediction model from the European Centre for Medium-Range Weather Forecasts (ECMWF), which provides a much larger sample of SSWs and allows us to address our research question with statistical confidence (Stockdale *et al.*, 2018; Johnson *et al.*, 2019). In other words, instead of using the model hindcasts to assess predictability, we use hindcasts as a data archive to understand the dynamical relationships (see also Byrne *et al.* (2019) for a similar approach). The assumption here is that the mechanism behind stratosphere–troposphere coupling is reasonably well represented in numerical weather prediction models, and therefore, the statistical surface response following SSWs should be similar in models and observations.

## 2 | DATA AND METHODS

### 2.1 | Data

We use the ERA5 reanalysis dataset provided by ECMWF as observations (Hersbach *et al.*, 2020). We use daily mean data from November 1981 to May 2019. The zonal wind velocity at 10 hPa is used to detect SSWs, and the zonal wind velocity at 850 hPa as well as total precipitation and 2-m temperature is used to describe their surface impacts. Moreover, geopotential height data at 1000 and 150 hPa are used to study the downward propagation of SSWs.

Given the incomplete sampling of SSWs in the observations, output of the same variables from ECMWF's seasonal forecasting model SEAS5 is further used (Stockdale *et al.*, 2018). Details of the model configurations are described in Johnson *et al.* (2019). We use the 12-hourly output within the extended winter season (November–April) from the re-forecasts initialized on the 1st of November of each year from 1981 to 2018, from which we form daily means. The dataset contains 51 ensemble members, thus providing 51 times more data over the same time period as compared to the observations. In our analyses, we focus on the SEAS5 output from December onward, such that the initial conditions play a minor role.

For all data, climatological anomalies are constructed by first removing the multi-year mean of each day. For SEAS5 data, the multi-year mean over all ensemble members is subtracted. Note that the multi-year mean is calculated for days of the same forecast lead time relative to the initialization date, thus resulting in 1-day shifted calendar days in March in leap years. The ERA5 dataset is interpolated from a native TL639 grid (average grid spacing of 30 km in the horizontal) onto the  $0.25^\circ$  latitude and  $0.25^\circ$  longitude grid. The SEAS5 precipitation and near-surface temperature data are interpolated from a native TCo319 grid (average grid spacing of 30 km in the horizontal) onto a  $1^\circ$  latitude and  $1^\circ$  longitude grid, and the wind and geopotential height data are interpolated onto a  $2.5^\circ$  latitude and  $2.5^\circ$  longitude grid.

## 2.2 | Methods

We use the commonly applied definition of Charlton and Polvani (2007) to define SSWs. Accordingly, an SSW is detected when the zonal-mean zonal wind at  $60^\circ\text{N}$  at 10 hPa from November to March is below  $0\text{ m}\cdot\text{s}^{-1}$ ; that is, the zonal-mean zonal wind is easterly (Charlton and Polvani, 2007). The first day this value becomes negative is called the central date of the SSW. This definition further requires that no other SSW is detected for at least 20 days after the winds have become positive again. This way, even if the winds become westerly for a few days, the same event is not counted twice. Finally, the definition requires that the zonal-mean zonal wind must return to positive for at least 10 consecutive days before April 30th to ensure that SSWs are not mistaken for the final warming of the polar vortex.

To explore a potential role of differences in the downward coupling of SSWs to the troposphere, the Northern Annular Mode (NAM) index is used. The NAM is calculated following Karpechko *et al.* (2017) as the area-weighted average of daily mean geopotential height over

the polar cap ( $60\text{--}90^\circ\text{N}$ ) for a given pressure level. The index is then standardized by subtracting the multi-year climatology of each day and dividing it by the daily multi-year standard deviation.

This standardized NAM index is used to classify SSWs into downward (dSSW) and non-downward (nSSW) propagating events (Karpechko *et al.*, 2017; White *et al.*, 2019). Following Karpechko *et al.* (2017), downward propagating events are those SSWs that fulfil the three following criteria: (1) the 1000 hPa NAM index (NAM1000) averaged over the 8–53 days after the SSW central date must be negative, (2) at least 50% of all days within this 8–53 period must have a negative NAM1000 value and (3) at least 70% of days within the 8–53 period must have a negative NAM150 value. Note that for the third criteria, we used the 150 hPa instead of the 100 hPa pressure level that was used in Karpechko *et al.* (2017), as the latter is not part of the SEAS5 output. According to White *et al.* (2019), the use of 150 hPa leads to similar results.

To address the role of sampling uncertainty, we use a bootstrap approach following Byrne *et al.* (2019). We generate 10,000 time series of length 38 years by randomly selecting one of the 51 ensemble members for each year. From these 10,000 time series, we then create a distribution of the studied characteristics (e.g., the number of SSWs per winter month) and compare it to the observations (Byrne *et al.*, 2019).

## 3 | RESULTS

### 3.1 | Model evaluation

To first evaluate how well SEAS5 is capable of simulating the SPV and its variability, we compare its key characteristics in the reanalysis with that of SEAS5. The SPV strength is here defined as the zonal-mean zonal wind velocity at  $60^\circ\text{N}$  at 10 hPa. Figure 1a shows the climatology (black thin line) as well as one and two standard deviations (SD, grey shadings) of the SPV over the course of the extended winter season. Strong westerly winds are observed during the winter that peak in January when vortex variability is also the largest. The winds then progressively slow down until turning, on average, negative in April. Similar characteristics can be seen in the SEAS5 model, overall giving a smoothed picture due to the larger number of data (Figure 1b). In contrast to ERA5, the climatological wind is strongest in December in the model.

We next calculate the number of SSWs per winter in both ERA5 and SEAS5 (Figure 1c). In total, 27 SSWs occurred during the 38 considered winters from

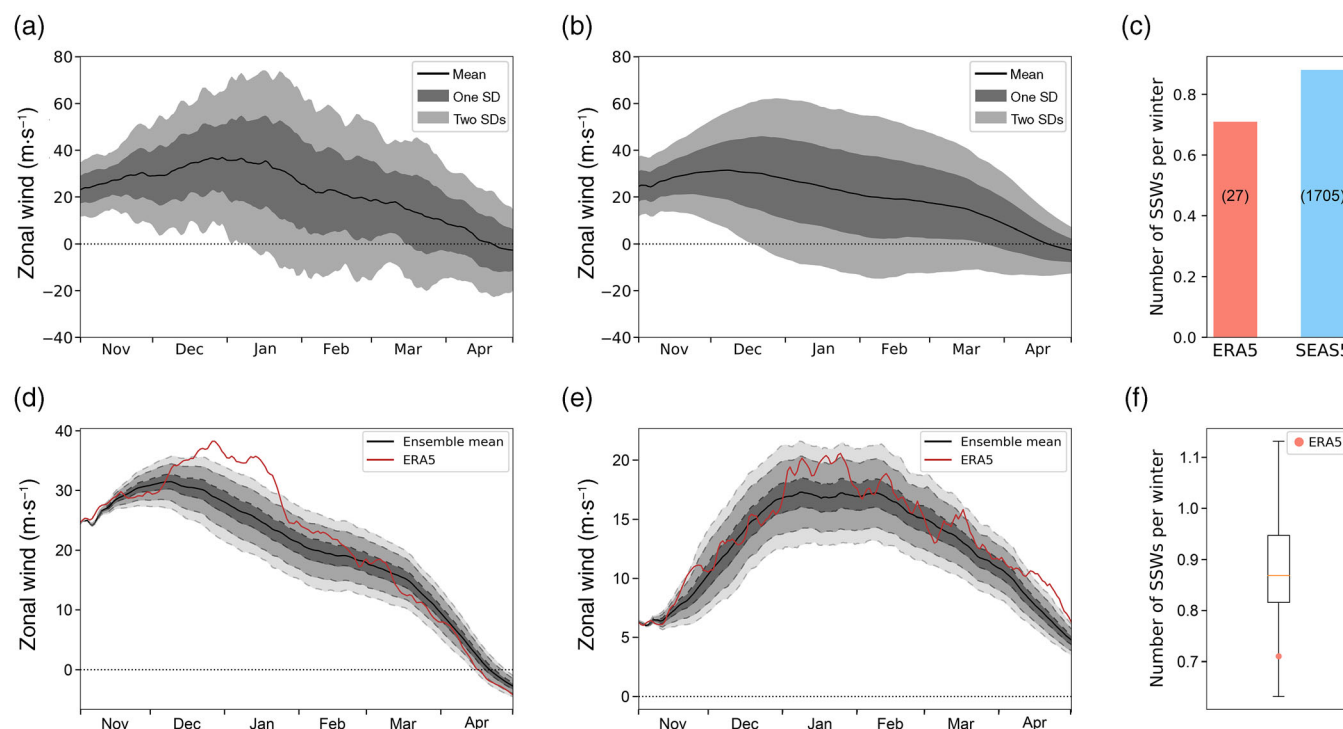


**FIGURE 1** Comparison between the SPV in the observational record (ERA5) and the model dataset (SEAS5). (a,b) Climatology of the SPV, defined as the zonal-mean zonal wind velocity at 60°N at 10 hPa (thin black line) for (a) ERA5 and (b) SEAS5, respectively. The dark and light grey shadings correspond to the one and two SDs. (c) Number of SSWs per winter for ERA5 (red) and SEAS5 (blue). The raw number of SSWs is indicated in brackets on the bars. (d) Bootstrap estimate of sampling uncertainty associated with 38-year mean of the SPV. The bootstrap estimate was generated using 10,000 time series of length 38 and randomly choosing one ensemble member for each year. Dashed lines represent the 1st, 5th, 25th, 75th, 95th and 99th percentiles. The red line corresponds to ERA5 observations. (e) The same as (d) but computing the SPV SD instead of the mean. (f) Number of SSWs per winter in the 10,000 time series. The orange line indicates the median, the box indicates the quartiles, and the whiskers show the 5th and 95th percentiles. The red dot indicates the observational value [Colour figure can be viewed at [wileyonlinelibrary.com](http://wileyonlinelibrary.com)]

November 1981 to April 2019 in the observational record, giving an average occurrence of 0.71 SSWs per winter. These events contain the same dates as the list of 23 major SSWs provided in Karpechko et al. (2017) based on Era-Interim data, with two additional events found on 17 February 2002 and 29 March 2008 in the ERA5 data set used here, as well as on 20 March 2018 and 1 January 2019, which occurred after the above study was published. In contrast, the 51 SEAS5 ensemble members contained 1705 events, giving an average of 0.88 SSWs per winter.

To understand the role of sampling variability in Figure 1a–c, we follow a bootstrap approach to create a distribution of 10,000 time series of length 38 years from the model ensemble and compare it to the observations (see also Section 2.2). We compute the mean (Figure 1d) and the SD (Figure 1e) of the SPV index over the course of the winter. The mean over all values is shown by the thin black line, while that of the observations is indicated in red. The grey shadings indicate the 1st, 5th, 25th, 75th, 95th and 99th percentile thresholds. While observed SPV

variability (red line in Figure 1e) is well within sampling uncertainty, the SPV mean in January lays outside the model spread (red line in Figure 1d), suggesting that the mean strength is underestimated by the model during this time. Moreover, we also compute the frequency of SSWs for all time series and show them in a box and whiskers plot with the observations again indicated in red (Figure 1f). Although the SSW frequency was found to be lower in the observations (Figure 1c), it is still consistent with sampling uncertainty. We further note that the weak bias in the model in January (Figure 1d) might contribute to the higher number of SSWs per winter in SEAS5, since their detection depends on the absolute threshold of  $0 \text{ m s}^{-1}$ . Overall, Figure 1 shows that despite these differences, the SPV seasonal evolution and variability, including SSW frequency, are well captured by SEAS5.

Next, we compare the surface impacts following SSWs in the model and the observations (Figure 2). We do this by plotting the zonal wind velocity anomalies at 850 hPa ( $u_{850}$ , Figure 2a,b), the precipitation anomalies (Figure 2c,d) and the near-surface temperature anomalies



(Figure 2e,f) averaged over the 30 days after the central date of all detected SSWs in the observations (Figure 2a,c, e) and in SEAS5 (Figure 2b,d,f). The observations show the expected negative NAO-type response. There are

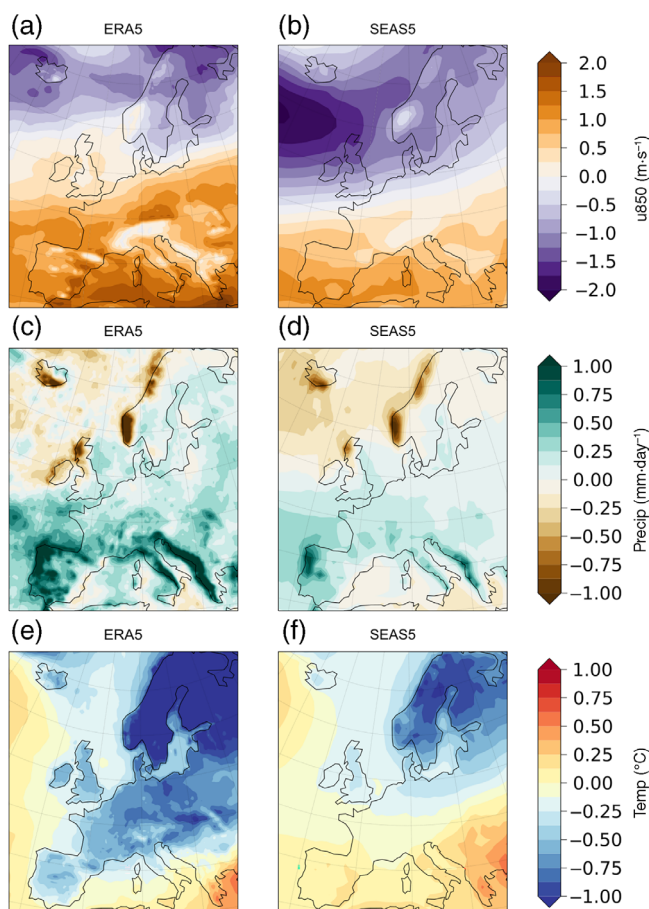


**FIGURE 2** Tropospheric response to SSWs. The panels show the 30-day averages of u850 (top row), precipitation (middle row) and temperature (bottom row) anomalies after the SSW central date, averaged over all SSWs in (a,c,e) ERA5 and (b,d,f) SEAS5 [Colour figure can be viewed at [wileyonlinelibrary.com](http://wileyonlinelibrary.com)]

negative wind anomalies over the North Atlantic and Scandinavia while wind anomalies over Southern Europe are positive (Figure 2a). This indicates southward shifted Atlantic storm tracks, transporting moist air to Southern Europe. Consistently, precipitation anomalies over Southern and Central Europe are anomalously high (Figure 2c). In particular, the Iberian Peninsula as well as Italy and the Balkan region show increased precipitation. In contrast, precipitation over Iceland, Ireland, Scotland and Norway is on average anomalously low in the months after a SSW. Temperature anomalies are negative, particularly over Scandinavia. Similar patterns are found in SEAS5 (Figure 2b,d,f). While negative wind anomalies over the North Atlantic following SSWs are more pronounced in the model (Figure 2b), associated precipitation anomalies are less extreme in SEAS5 (Figure 2d). Moreover, colder than average temperatures are mostly confined to Northern Europe in SEAS5 (cf. Figure 2e,f). Differences in the response might at least partly be related to the higher numbers of events in the model compared to the observations, which will tend to blur the effects of individual events. Moreover, it is possible that some of the differences between SEAS5 and ERA5 are due to a better resolved orography in ERA5 (as it has higher spectral resolution than SEAS5).

In summary, Figures 1 and 2 show that SEAS5 depicts polar vortex variability and the surface weather impacts following SSWs reasonably well. This justifies our approach to use the SEAS5 model data to study the role of SSW timing on precipitation impacts over Europe.

### 3.2 | The role of SSW timing on the surface response

To investigate the role of the SSW timing on European precipitation, we first study the monthly distribution of

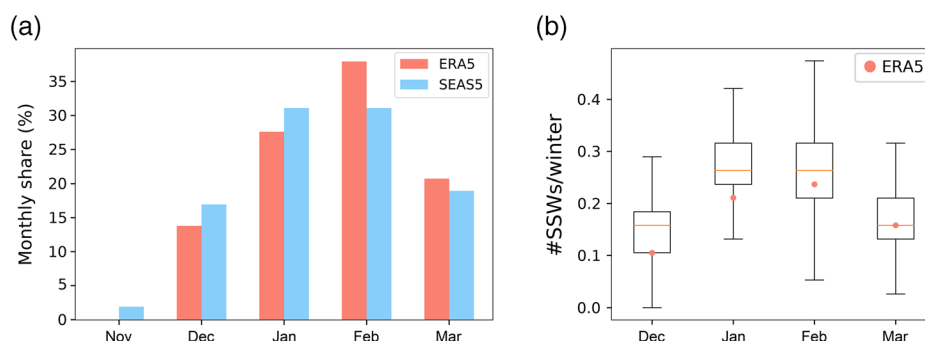


**FIGURE 3** Representation of the SSW timing. (a) Number of SSWs per month, shown as a fraction of all the events for ERA5 (red) and SEAS5 (blue) for each month of the winter season. (b) Distribution of the number of SSWs per winter month, calculated for the 10,000 model time series. The orange lines indicate the median, the boxes indicate the quartiles, and the whiskers show the 5th and 95th percentiles. The red dots are the observed values [Colour figure can be viewed at [wileyonlinelibrary.com](http://wileyonlinelibrary.com)]

the frequency of SSWs. Figure 3a shows the percentage of SSWs that occurred in a given winter month, both for ERA5 (in red) and SEAS5 (in blue). We find that SSWs are more likely to occur in January and February (for ERA5 27% and 38% of all events) and less likely to occur in December and March (for ERA5 13% and 20% of all events) both in the observations (ERA5) and in the model (SEAS5). Unlike the observations, SEAS5 contains a few events in November that we ignore in the following (see also Section 2.1).

As before, the role of sampling uncertainty on the monthly occurrence rates is studied using a bootstrap approach. Figure 3b shows the number of SSWs per month per winter in the 10,000 time series using box and whiskers plots, with the observations indicated in red. On average, there are roughly as many SSWs in January as in February, and as many in December as in March, with

the latter group having much lower numbers of events than the former, consistent with Figure 3a. Furthermore, we note that the observations lie in the second quartile in December, February and March, and slightly below in January. Thus, the differences between the model and the observations are again consistent with sampling variability.

Similar to Figure 2b,d,f, we plot the u850, precipitation and temperature anomalies in SEAS5, averaged over the 30 days after the SSW central date, this time separately for each month of SSW occurrence (Figure 4). The canonical negative NAO-type response is found for each month. That is, there are, on average, windier and wetter weather conditions in Southern Europe, while Northern Europe experiences less wind and rain but overall colder temperatures. Interestingly, the strength of the anomalies weakens as the winter season progresses. While early

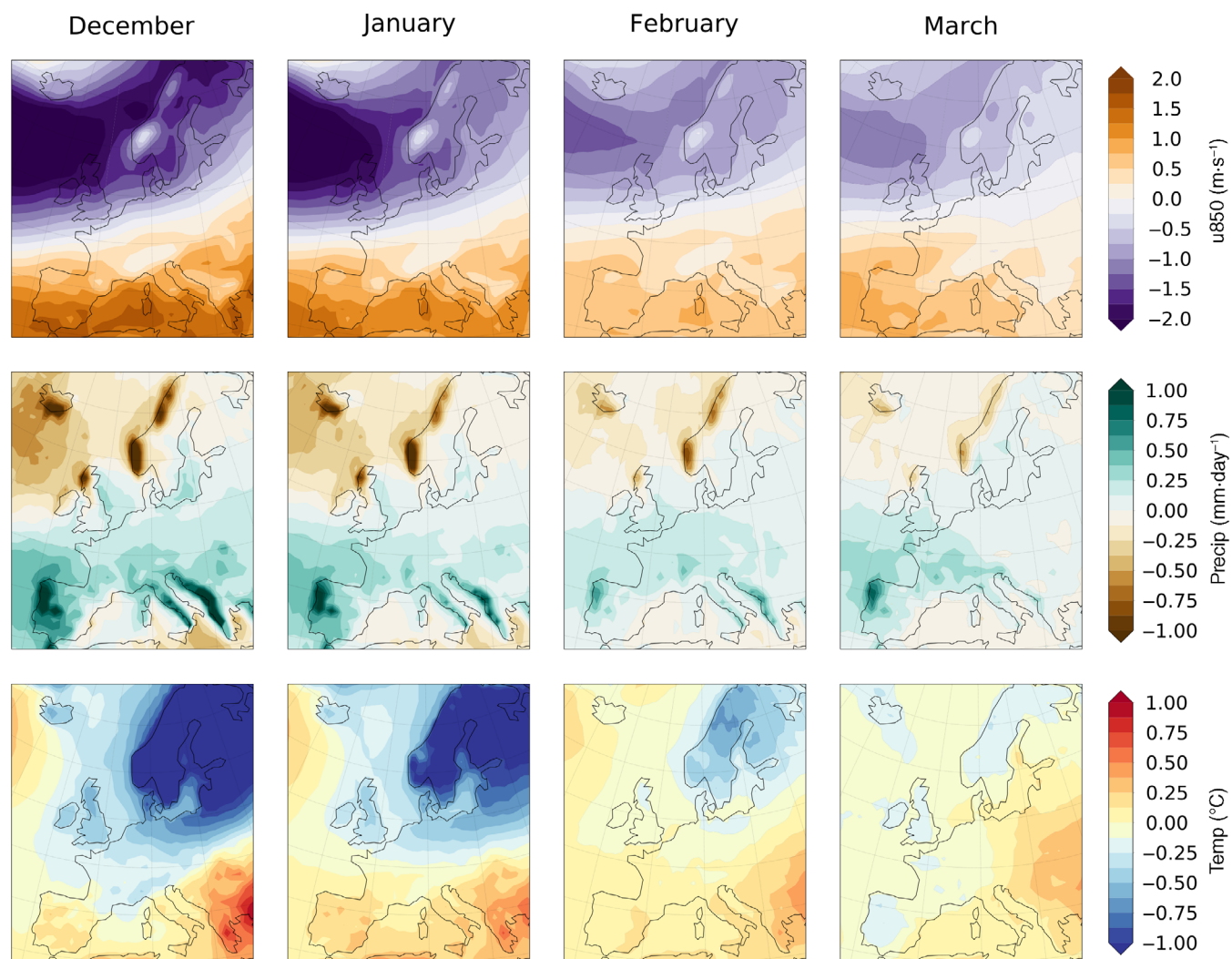


**FIGURE 4** Tropospheric response to SSWs split by month. Shown are 30-day averages of u850 (top row), precipitation (middle row) and temperature (bottom row) anomalies after the SSW central date for each month in the winter season for SEAS5 [Colour figure can be viewed at [wileyonlinelibrary.com](http://wileyonlinelibrary.com)]



winter (December and January, DJ) events are followed by strong u850, precipitation and temperature anomalies, the response is less pronounced in late winter (February and March, FM). For example, while average precipitation anomalies over the Balkans in the month after an SSW occurring in December exceed  $1 \text{ mm} \cdot \text{day}^{-1}$ , they are close to climatology after March SSWs. Similarly, rainfall is strongly decreased over Scotland after early winter SSWs, while the signal is only weak after late winter events. For temperatures, the difference is especially pronounced over Norway, where December SSWs are associated with temperature anomalies of  $-1.3^\circ\text{C}$ , whereas they only reach  $-0.2^\circ\text{C}$  during SSWs occurring in March.

To investigate the difference between early and late winter SSWs in more detail, we compute regional indices of precipitation anomalies for four regions particularly affected by SSWs (see Figure 5a). We follow King *et al.* (2019) and consider precipitation and temperature anomalies in Iberia and Eastern Europe (which are both associated with anomalously high precipitation and temperatures after SSWs in SEAS5), as well as over Scotland and Norway (which are both associated with anomalously low precipitation and temperatures after SSWs). Note that the latter two regions are here smaller than the regions considered by King *et al.* (2019). Figure 5b shows the 30-day average following SSWs for each region and month, normalized by the multi-year average of the month of the central date of the SSWs. That is, precipitation anomalies following SSWs occurring in December are divided by the December precipitation climatology and so forth. Consistent with Figure 4, the regional anomalies following SSWs—now expressed as percentages of the monthly climatology—decrease over the course of the winter. For example, after SSWs occurring in December, there is, on average, 17% more precipitation in Iberia and 15% in Eastern Europe, compared to their

December climatology. In contrast, SSWs occurring in March only show an increase in 8.7% and 2.4%, respectively, of the climatology of that month. Similarly, the anomalously low precipitation in Scotland and Norway decreases from 5.5% and 12% after December SSWs to just 1.5% and 3.6%, respectively, after SSWs occurring in March. This means that the results in Figure 4 are not due to overall lower precipitation climatologies in late winter. These findings are also robust (not shown) when normalizing the precipitation anomalies by the 15 days shifted monthly average (i.e., calculated from the 15th of the month of the central date up to the 15th of the following month), to account for the fact that precipitation composites following SSWs also include days outside of the month of the central date. We further plot the regional temperature anomalies (Figure 5c) and find a similar pattern. In all considered regions, early winter SSWs are associated with more pronounced temperature anomalies than late winter SSWs. This difference is particularly striking over Norway.

We test how these findings compare to the observations, including whether the results are consistent within sampling variability using a bootstrap approach. Figure 6 shows the observed precipitation (expressed as percentages) and temperature anomalies in the four different regions after early (DJ, dark blue bars) and late winter (FM, yellow bars) SSWs. We reduce our analysis to early and late winter events here, to increase the analysed sample size of the observations. Except for Iberia, precipitation anomalies in ERA5 are more pronounced after early winter SSWs (see Figure 6a), consistent with Figures 4 and 5. For observed temperatures, qualitatively similar differences between early and later winter SSWs are found for Norway and Iberia but not for Scotland and Eastern Europe. Given the noise in the observations, some inconsistency is to be expected. We further address

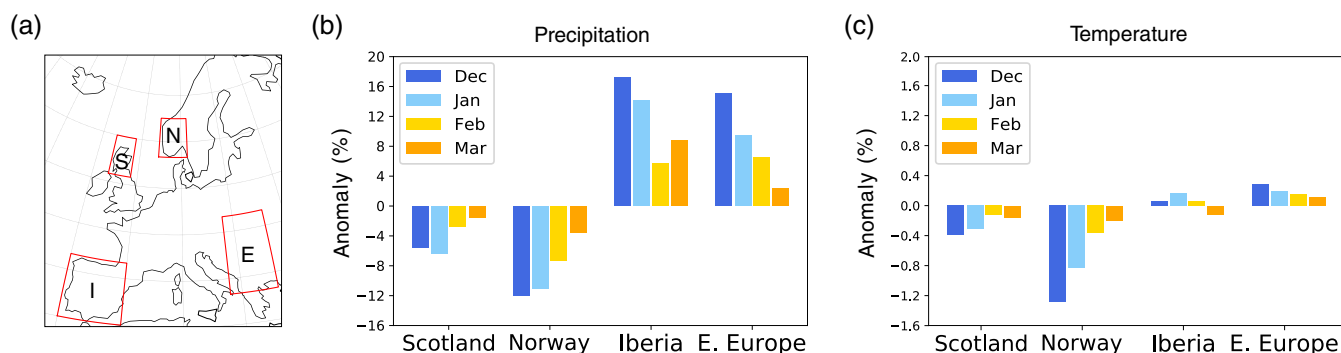


**FIGURE 5** Regional precipitation anomalies. (a) Map of Europe showing the four regions (red rectangles) over which regional indices are calculated: Scotland ( $6.5\text{--}1.5^\circ\text{W}$ ,  $55\text{--}60^\circ\text{N}$ ), Norway ( $4.5\text{--}11.5^\circ\text{E}$ ,  $58\text{--}63^\circ\text{N}$ ), Iberia ( $10^\circ\text{W}\text{--}1^\circ\text{E}$ ,  $36\text{--}44^\circ\text{N}$ ) and Eastern Europe ( $18\text{--}26^\circ\text{E}$ ,  $40\text{--}50^\circ\text{N}$ ). (b) Thirty-day averaged precipitation anomalies following SSWs normalized by the multi-year monthly climatology, for each region and each month of the winter season. (c) Thirty-day averaged temperature anomalies following SSWs, for each region and each month of the winter season [Colour figure can be viewed at [wileyonlinelibrary.com](http://wileyonlinelibrary.com)]

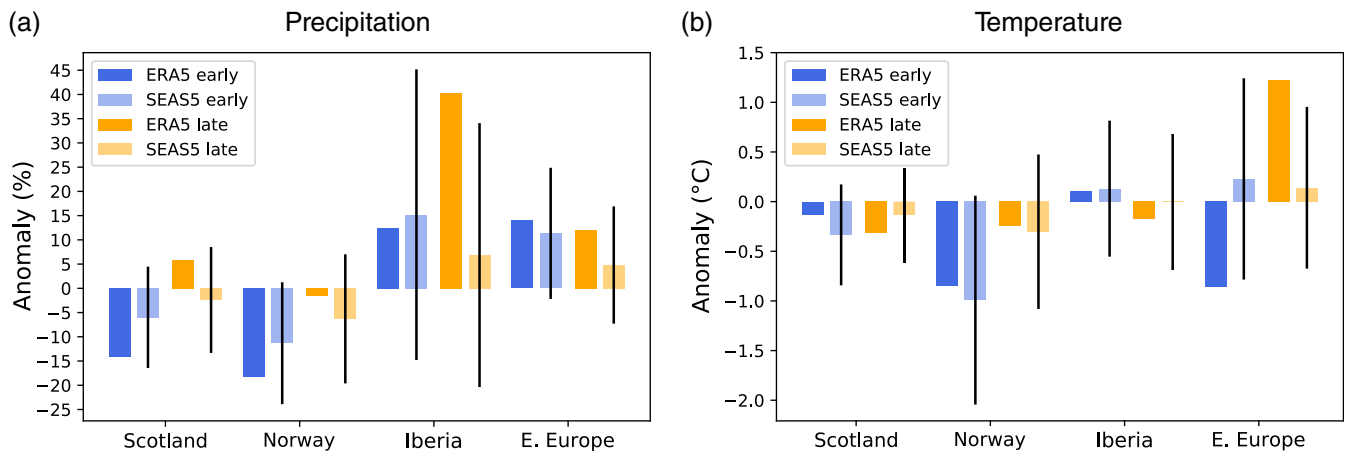


**FIGURE 6** Consistency with the observations and the role of sampling uncertainty. Thirty-day averaged anomalies following SSWs for each region and split by early or late winter occurrence for (a) precipitation (normalized by the multi-year early [DJ] and late winter [FM] climatology) and (b) temperature. The observations are shown by the dark blue and yellow bars. The light blue and orange bars show the results for the model, with the height of the bars indicating the median of the 10,000 time series (see Section 2.2) and the black lines indicating the 5th and 95th percentile [Colour figure can be viewed at [wileyonlinelibrary.com](http://wileyonlinelibrary.com)]

this by showing the median precipitation and temperature anomaly for the 10,000 time series in SEAS5 (light blue and orange bars in Figure 6), with the black lines indicating the 5th and 95th confidence interval. While observed results for precipitation in Scotland, Norway and Eastern Europe, as well as early winter results for Iberia are well within sampling variability, the late winter SSW response for Iberia is not. Note, however, that the confidence interval is widest for this region, indicating that sampling variability can at least somewhat contribute to this difference. For Scotland and Norway, observed differences between early and late winter SSWs are even more pronounced than in the model. For anomalous temperatures, the observed early and later winter anomalies are also within sampling uncertainty, except for Eastern Europe where the observed values lie just outside the range. Overall, despite the outlier of Iberian precipitation after late winter SSWs, and temperatures in Eastern Europe, the observed precipitation and temperature response following early and late winter SSWs is mostly consistent with SEAS5. Recall that the confidence intervals are on the subsamples representative of the observations, just as in Figures 1d–f and 3b, indicating that the observations are consistent with the behaviour we see in the model.

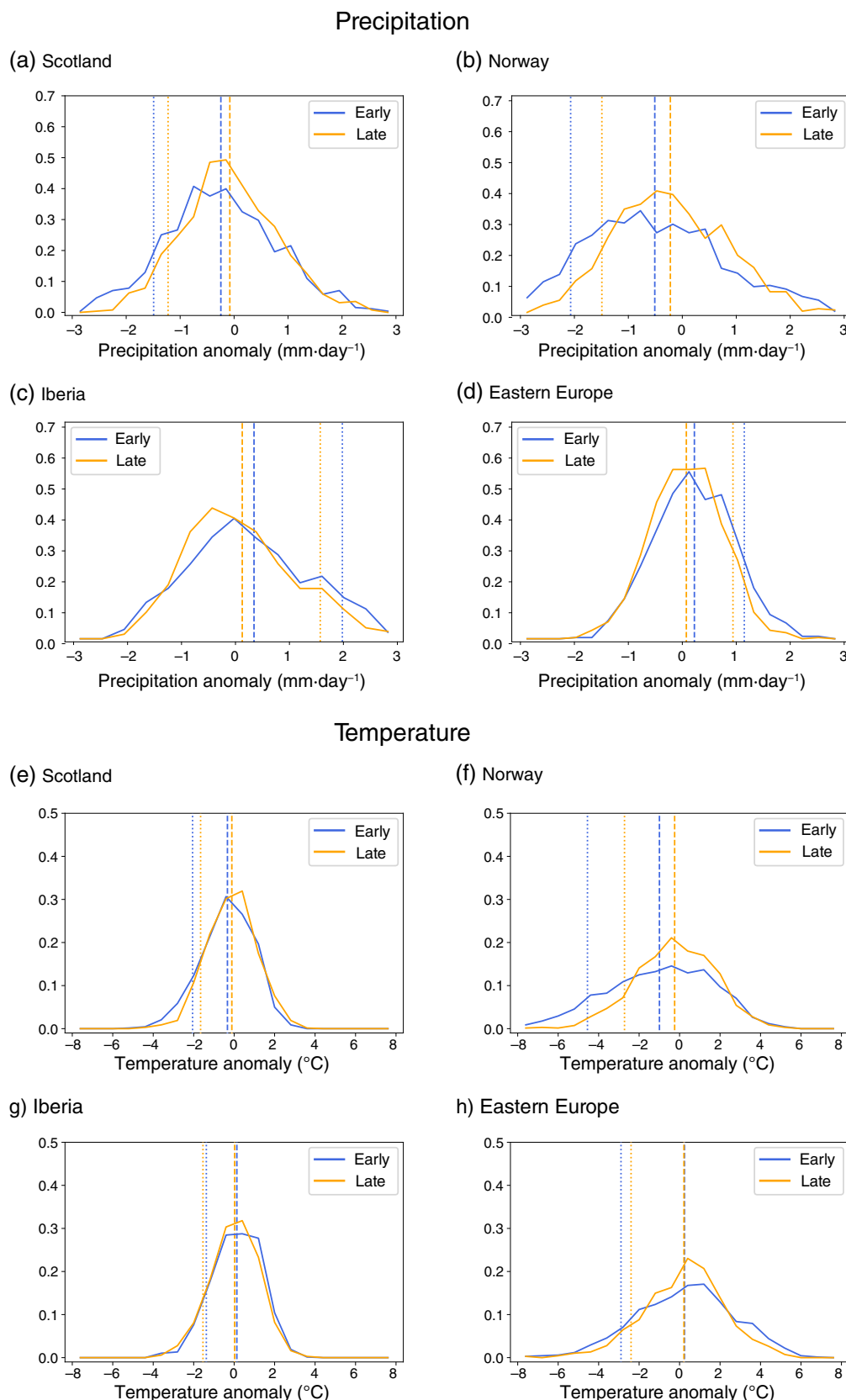
### 3.3 | Regional risk of extreme events

We further address how the timing of SSWs is related to the occurrence of extreme events. For consistency with the previous results, we again analyse the 30-day averaged precipitation and temperature anomalies after

SSWs. Figure 7 shows the probability density function of such anomalies for early winter (blue) and late winter (orange) SSWs. The respective means are indicated by the dashed lines, and extreme percentiles of precipitation (10st for the British Isles and Southern Scandinavia, and 90st for Iberia and Eastern Europe) are shown by the dotted lines. Clearly, not only are the means of early winter values separated in all regions, coherent with our previous findings (Figures 4 and 5), but also the extreme values are more pronounced in each region after early winter SSWs. These results are also consistent with those of King *et al.* (2019) for the observations.

To better quantify the risk of extreme events following early and late winter SSWs, we further compute the risk ratios for each region. In order to do so, we computed the top and bottom 10% extreme 30-day averaged precipitation and temperature anomalies for each region. The risk ratio is the probability of an extreme event occurring after the central date of an early winter SSWs, divided by the probability of it occurring after late winter SSWs. Here, we find risk ratios of extremely low precipitation (below the 10th percentile) of 1.7 Scotland and of 2.6 for Norway. This means, for example, that the risk of extremely dry conditions is more than doubled in Norway after the occurrence of an early winter SSW compared to that of a late winter SSW. Consistently, we find risk ratios of extremely high precipitation (above the 90th percentile) of 1.7 both for Iberia and for Eastern Europe. Risk ratios for extremely low temperatures in Scotland and Norway are 1.1 and 1.4, while that of extreme high temperatures in Iberia and Eastern Europe are 1 and 1.5. Thus, consistent with the previous analysis, the risk of extreme anomalous precipitation is roughly increased by a factor of 2 after early winter SSWs

**FIGURE 7** Probability density functions of 30-days averaged precipitation anomalies following early winter SSWs (blue) and late winter SSWs (orange) for (a) Scotland, (b) Norway, (c) Iberia and (d) Eastern Europe (see Figure 5 for details on the regions). The dashed lines show the average precipitation anomalies, and the dotted lines show the (a,b) 10th and (c,d) 90th percentiles. (e–h) The same as (a–d) but for temperature anomalies instead of temperature [Colour figure can be viewed at [wileyonlinelibrary.com](http://wileyonlinelibrary.com)]



compared to that of late winter SSWs. For extreme temperatures, the risk is also increased (except for Eastern Europe) but is less pronounced. Note that the risk of extreme events occurring in the month after the central date of SSWs

(regardless of month of occurrence) compared to months with no SSWs are of comparable magnitude or even smaller (for extreme precipitation, the risk ratios are 0.8 and 1.1 for Scotland and Norway, and 1.5 and 1.3 for Iberia and

Eastern Europe; for extreme temperature, the risk ratios are 1.2 and 1.4 for Scotland and Norway, and 1 and 1.2 for Iberia and Eastern Europe).

### 3.4 | Are there more downward propagating SSWs in early winter?

We now investigate a potential dynamical explanation for this difference between the early and late winter SSW response. More precisely, we test if there are more SSWs

that are downward propagating to the troposphere in early winter than in late winter. This could explain the more pronounced surface response in early winter, as downward propagating SSWs show by definition a stronger response in the tropospheric circulation (Karpechko *et al.*, 2017). To test this hypothesis, we categorize each SSW into either downward propagating (dSSWs) or non-downward propagating SSWs (nSSWs) (see Section 2.2). We then first evaluate how well these properties are captured by the model. To do this, we plot the monthly share of dSSWs for both ERA5 and SEAS5 (see dashed line in

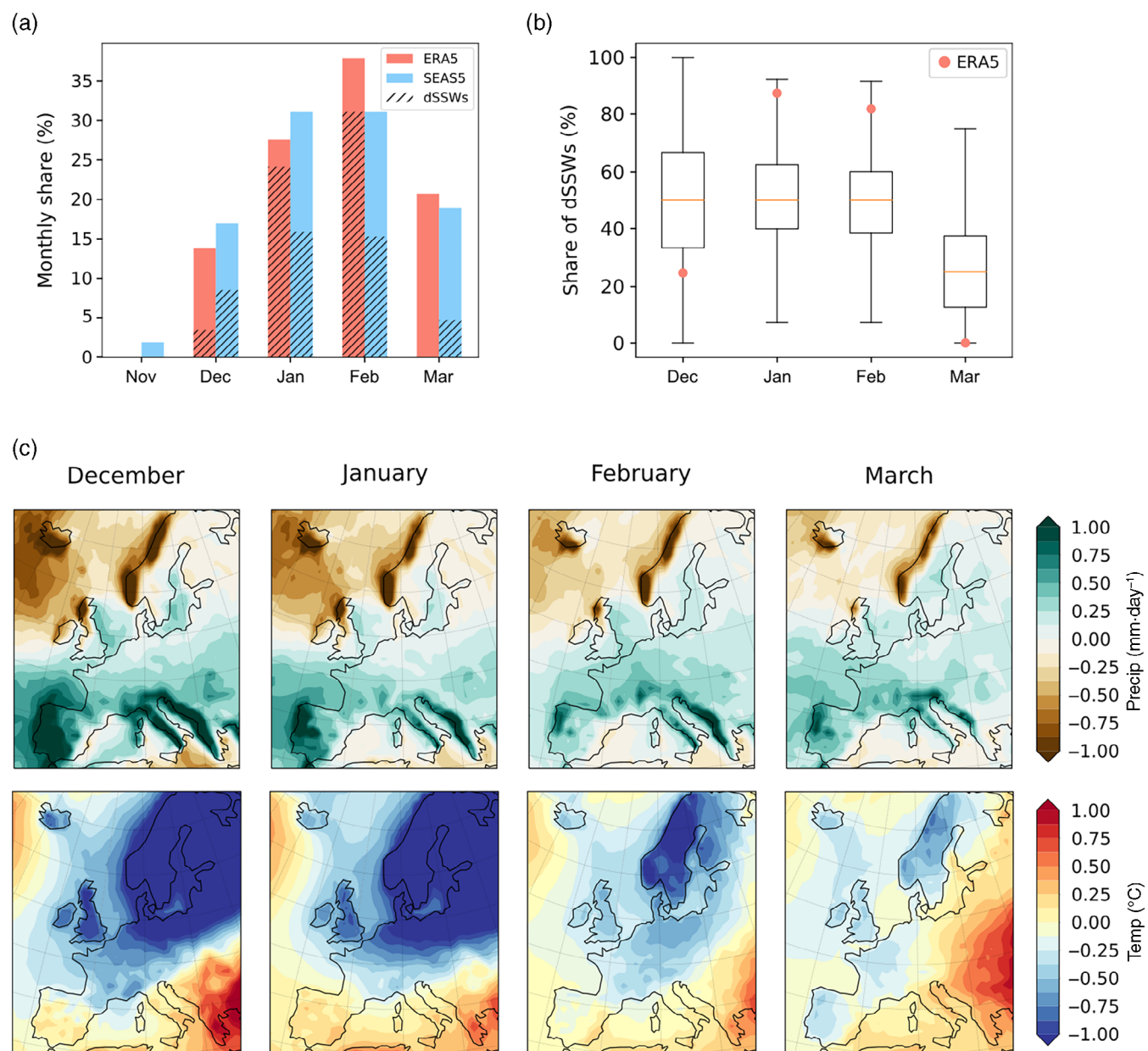


**FIGURE 8** The role of downward propagation of SSWs (dSSWs). (a) Proportion of dSSWs per month (dashed) for ERA5 (red) and SEAS5 (blue) for each month in winter. (b) Share of dSSWs of all SSWs per month in the 10,000 model time series. Orange lines are the medians over all time series. Red dots are the observed values. The whiskers indicate the 5th and 95th percentiles. (c) The same as in Figure 4 but for dSSWs in SEAS5 only [Colour figure can be viewed at [wileyonlinelibrary.com](http://wileyonlinelibrary.com)]



Figure 8a) and again address the role of sampling uncertainty of this ratio using a bootstrap approach as before (Figure 8b). We make two observations.

First, we find that there are more dSSWs in the observations than in SEAS5. In Figure 8a, only half of January and February SSWs are downward propagating in the model, while more than 80% of those in the observations are dSSWs. In contrast, the share of dSSWs in December in the model is twice as large as that in the observations. Furthermore, there are some detected dSSWs in March in SEAS5 while there are none in ERA5. The box and whiskers plots in Figure 8b show that these rather strong differences are yet still consistent with sampling uncertainty, albeit being on the outer edges of the distributions.

Second, Figure 8a shows that there is no clear difference in the number of dSSWs occurring in early and late winter. In fact, the percentage of dSSWs in SEAS5 in early winter (24% of all events) is approximately the same as in late winter (20%). Thus, the ratio of dSSWs cannot explain the difference between the early (DJ) and late winter (FM) SSW responses shown in Figure 4. To confirm this, we also plot the precipitation and temperature anomalies in the 30 days following only the dSSWs for each month of the winter period (Figure 8c). By construction, the precipitation and temperature anomalies are now much more pronounced, as only the stratospheric events that reach the troposphere are included. However, we still find that the anomalies are weaker after late winter SSWs. This confirms a role of the timing of SSWs for their precipitation response that cannot be explained by different numbers of downward propagating SSW events.

### 3.5 | The role of the stratospheric mean state and event definition

Finally, we assess the role of the stratospheric state in explaining the surface differences. We plot for each winter month the SPV strength anomaly (measured as the zonal-mean zonal wind anomaly at 60°N at 10 hPa) during the central date of SSWs, against the associated surface response, here measured in terms of the (non-standardized) NAM1000 index averaged 30 days after the central date of the SSW. The scatter plot of the two quantities (see Figure 9a) indicates an almost perfect linear dependence ( $r = .99$ ,  $p < .01$ , according to a two-sided Student's  $t$  test). We repeat the analyses using the regional temperature and precipitation anomalies instead of the NAM1000 (not shown) and report consistently high and statistically significant correlations (ranging from  $r = -.69$  for Iberian temperatures to  $r = .98$  for

precipitation in Norway). Thus, the different monthly averaged NAM1000 responses (and consistently the precipitation and temperature anomalies) can entirely be explained by differences in the strength of the stratospheric wind anomalies, with early winter SSWs being on average associated with much stronger wind anomalies ( $-32 \text{ m}\cdot\text{s}^{-1}$  in December,  $-26 \text{ m}\cdot\text{s}^{-1}$  in January) than later winter SSWs ( $-22 \text{ m}\cdot\text{s}^{-1}$  in February,  $-16 \text{ m}\cdot\text{s}^{-1}$  in March). In other words, the stronger the stratospheric forcing, the stronger the surface response. While some previous studies concluded that the surface response to SSWs does not correlate with the strength of mid- and upper stratospheric anomalies (Runde *et al.*, 2016; Karpechko *et al.*, 2017), a similar dependence on the strength of the stratospheric anomalies was also found in Polichtchouk *et al.* (2018a, 2018b) who varied the parametrized non-orographic gravity wave drag strength in the ECMWF model. Furthermore, a dependence between tropospheric circulation anomaly and precipitation anomaly has been reported (Zappa *et al.*, 2015; Bevacqua *et al.*, 2021), consistent with our results.

We argue that while the relationship between SPV and NAM1000 anomalies is physical, the stronger SPV anomalies during early winter SSWs (Figure 9a) are a statistical artefact, directly related to the SSW event criterion. Recall that a day is classified as a SSW when the stratospheric zonal-mean zonal wind surpasses the *absolute* threshold of  $0 \text{ m}\cdot\text{s}^{-1}$ . However, the stratospheric mean state is stronger in early than in late winter (see also black line in Figure 1b). Thus, by selecting only those days where winds are below  $0 \text{ m}\cdot\text{s}^{-1}$ , early winter events will have stronger wind *anomalies* (relative to the climatological mean state). To test and visualize this effect, we first plot the daily SPV anomaly against the (30-day averaged) NAM1000 anomalies for all winter days and find, as expected, a statistically significant correlation (Figure 9b,  $r = .24$ ,  $p < .01$ ). Importantly, there is, also as expected, no dependence on the winter months (indicated by the different colours in the scatter plot), with anomalies spread similarly across the different months (cf. Figure 1b). In contrast, when we compute the same plot for SSWs only, we find a clear separation between the winter months, with the early winter SSWs (blue dots in Figure 9c) showing much stronger SPV anomalies and, therefore, NAM1000 anomalies.

In statistics, the effect discussed above is known as a selection or collider bias and can be identified with a causal network (Kretschmer *et al.*, 2021). The network in this case (Figure 9d) illustrates the assumed causal, that is, physical, dependencies with the circles representing the involved variables and the arrows indicating the presence and direction of an assumed causal influence. Here, we assume a causal chain from 'SPV anomaly' to



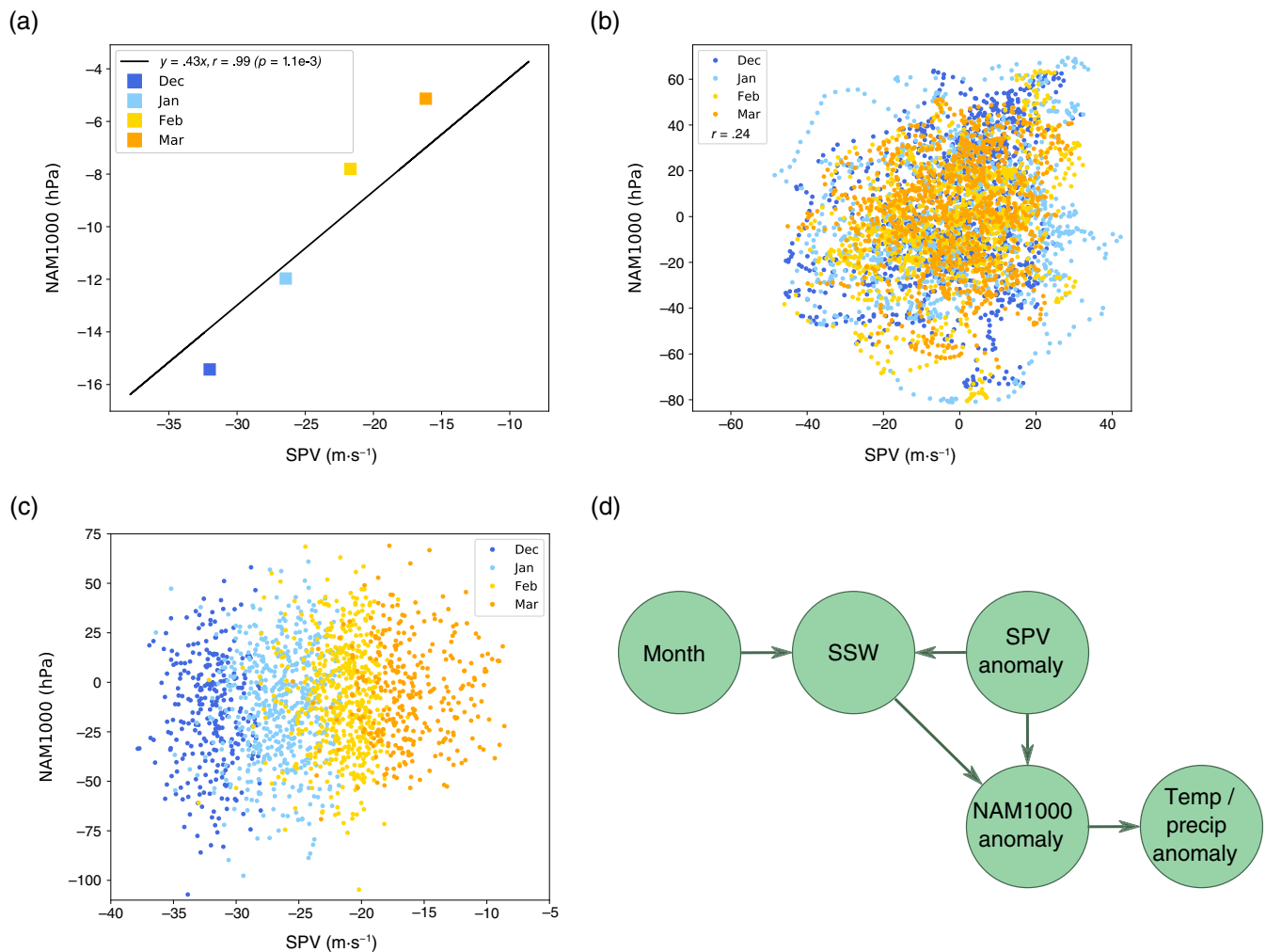


**FIGURE 9** The role of the stratospheric state. (a) Scatter plot of the SPV anomaly during the central date of SSWs for each month and according to the (non-standardized) NAM1000 anomaly averaged 30 days after the central dates in SEAS5. The black line indicated the regression line resulting from fitting  $y = \text{NAM1000}$  on  $x = \text{SPV}$ . (b) Scatter plot of SPV anomalies during all winter days and the according (non-standardized) NAM1000 anomalies averaged in the following 30 days. The different colours indicate the different winter months, see legend. To aid visualization, we only show SPV and NAM1000 anomalies of the first ensemble member. (c) The same as (b) but for SSWs only and using all ensemble members. (d) The causal network representing the involved causal dependencies. The SPV anomaly is assumed to affect the NAM1000 anomaly, which affects the temperature and precipitation anomaly in Europe. SSWs are defined as when the zonal-mean zonal wind anomaly is negative, with the strength of the mean-state varying across the winter. Therefore, the occurrence of an SSW is influenced both by the SPV anomaly as well as the month. Just as SPV anomalies in general, SSWs also affect the NAM1000 anomaly [Colour figure can be viewed at [wileyonlinelibrary.com](http://wileyonlinelibrary.com)]

‘NAM1000 anomaly’ and further to ‘temperature/precipitation anomaly’. Moreover, as argued before, both ‘SPV anomaly’ and ‘month’ affect the selection of ‘SSW’, which, in turn, affects ‘NAM1000 anomaly’. The variable ‘SSW’ is, hence, a common effect (also called a collider) of ‘SPV anomaly’ and ‘month’, which are, otherwise, not statistically associated (see Figure 9b). By conditioning on, that is, selecting the common effect ‘SSW’, a spurious association between ‘month’ and ‘SPV anomaly’ is introduced (see Figure 9c).

In summary, while there is considerable spread across individual events (Figure 9c), differences in the

SPV anomalies during SSWs in the winter months can fully explain the differences in the surface impacts (Figure 9a). The different SPV anomalies arise from the event definition of SSWs, which does not account for different mean states in the winter months.

## 4 | DISCUSSION

Our results suggest that the timing of SSWs plays an important role for their surface impacts, with early winter SSWs being followed on average by stronger

precipitation and temperature anomalies compared to late winter SSWs. Here, we tested if the number of downward propagating SSWs can explain the different precipitation anomalies, but found this not to be the case. Similarly, the seasonal evolution of climatological precipitation cannot explain the differences.

Instead, a simple explanation for the surface differences of SSWs can be given by differences in the SPV anomaly in different winter months, thus by the strength of the stratospheric forcing. Differences in the forcing (and thereby the surface response) are a statistical artefact that is directly related to the event definition of SSWs, which involves an absolute threshold (of  $0 \text{ m s}^{-1}$ ), resulting in stronger SPV anomalies during early winter events, where the stratospheric mean state is stronger.

Thus, caution is needed when interpreting surface impacts following SSWs (defined using an absolute threshold) as, by construction, event composites will be dominated by the early winter events. Moreover, deficits in climate models in capturing SSW frequencies may be related to the stratospheric mean state being misrepresented (Polichtchouk *et al.*, 2018b). In a similar manner, changes in SSW frequency under global warming can be the result of changes in the mean state and not that of changes in the vertical wave activity (McLandress and Shepherd, 2009). These examples stress why using *relative* event criteria to study stratospheric extreme events can be beneficial (Hitchcock *et al.*, 2013; Kretschmer *et al.*, 2018a; Baldwin *et al.*, 2020). Nevertheless, there is, of course, a physical basis for an absolute criterion, with the  $0 \text{ m s}^{-1}$  threshold implying that planetary waves (and stationary orographic gravity waves) can no longer propagate into the stratosphere, thus changing stratospheric dynamics. The appropriate event definition, therefore, depends on the guiding research question, and it is important to bear both the physical and statistical characteristics of each in mind.

More generally, this study contributes to a larger body of literature arguing that seasonal-mean analyses of teleconnections, and of stratosphere–troposphere coupling in particular, can blur over important details (Jiménez-Esteve and Domeisen, 2018; Kretschmer *et al.*, 2018a; King *et al.*, 2021). While differences in the monthly surface response to SSWs were here demonstrated to be the result of the SSW definition, other teleconnections and their seasonal dependencies might give further insights into European climate variability. For example, the influence of La Niña on the NAO is mostly observed during February but not during the other winter months (Jiménez-Esteve and Domeisen, 2018). Similarly, the North Atlantic response to ENSO in late autumn was proposed to be different compared to mid-winter (King *et al.*, 2021). Understanding how these other mechanisms are related to our findings and contribute to differences in

the surface response to SSWs is important but is beyond the scope of the present study.

Finally, we note that although we found SEAS5 to reasonably well represent SSW frequency and downward coupling characteristics, we cannot make direct inferences concerning the real world because of sampling limitations in the observed record. For example, model biases (Tietsche *et al.*, 2020), as, for example, in the SPV strength for January in SEAS5, might affect our results. Additional analysis showed that this bias in January was not present in the SEAS5 data initialized on the 1st of December (not shown). The observed increased precipitation in Iberia and high temperature anomalies in Eastern Europe after late winter SSWs were more pronounced than in the model but the reasons for that were not investigated here. Testing our findings in other models and for shorter lead times, for example, such as in models participating in the S2S project (Vitart and Robertson, 2018), is, therefore, an important next step.

## 5 | SUMMARY AND CONCLUSIONS

SSWs strongly impact European winter weather. This study analysed the role played by the timing of SSWs within the winter season on the precipitation and temperature response over Europe. To address this question, we capitalized on the large ensemble hindcasts of the ECMWF seasonal forecast model SEAS5 initialized on the 1st of November of each year, providing a bigger archive of SSWs.

We analysed how well the model captures key stratospheric characteristics such as mean stratospheric wind velocity and variability (Figure 1), average frequency of SSWs (Figure 3) as well as the number of downward propagating SSWs (Figure 8a,b), and found the model to reasonably capture the expected properties, with differences from the observations being mostly within sampling uncertainty. Moreover, we tested how well the precipitation, temperature and zonal wind velocities at 850 hPa after SSWs in the model resembled those in the observations (Figure 2). While there were some differences, in particular, regarding the North Atlantic wind anomalies, overall, we found the model to well represent the surface impacts related to SSWs.

The analysis of the timing in SEAS5 suggested a difference between early (DJ) and late (FM) winter events. We found that early winter SSWs have a stronger impact on European weather, with higher precipitation and temperature anomalies (Figures 4 and 5). In contrast, late winter events have a smaller influence on surface weather. For example, while precipitation after December SSWs in Norway is reduced by approximately

12% of the monthly climatology, a reduction of only 4% was found after SSWs occurring in March. Except for Iberia, these results are consistent with the observed response of SSWs, despite the limited sample size (Figure 6). Consistently, the risk of extreme precipitation anomalies and similarly that of extreme temperature anomalies in the month after the occurrence of SSWs is increased after early winter SSWs (Figure 7).

We showed that this difference between early and late winter events cannot be explained by a different number of downward propagating SSWs, which were here found to be similar for early and later winter (Figure 8). Instead, differences are the result of the commonly used SSW event definition that involves an absolute threshold, thereby favouring stronger events (in terms of anomalous SPV strength) in early winter when the stratospheric mean state is stronger (Figure 9). Overall, this study, thus, demonstrates the role of SSW event definition in affecting surface impacts.

## ACKNOWLEDGEMENTS


The authors thank Ted Shepherd and Emanuele Bevacqua for useful feedback and discussions. They further thank two anonymous reviewers for constructive feedback, which helped to improve the manuscript.

## AUTHOR CONTRIBUTIONS

**Erika Monnin:** Conceptualization; formal analysis; investigation; visualization; writing – original draft; writing – review and editing. **Marlene Kretschmer:** Conceptualization; data curation; investigation; project administration; supervision; writing – original draft; writing – review and editing. **Inna Polichtchouk:** Conceptualization; writing – original draft; writing – review and editing.

## ORCID

Marlene Kretschmer  <https://orcid.org/0000-0002-2756-9526>

Inna Polichtchouk  <https://orcid.org/0000-0002-8943-4993>

## TWITTER

Marlene Kretschmer  @Marlene\_Climate

## REFERENCES

- Afargan-Gerstman, H. and Domeisen, D.I.V. (2020) Pacific modulation of the North Atlantic storm track response to sudden stratospheric warming events. *Geophysical Research Letters*. Blackwell Publishing Ltd, 47(2). <https://doi.org/10.1029/2019GL085007>.
- Ayarzagüena, B., Barriopedro, D., Garrido-Perez, J.M., Abalos, M. and Ordóñez, C. (2018) Stratospheric connection to the abrupt end of the 2016/2017 Iberian drought. *Geophysical Research Letters*. Blackwell Publishing Ltd, 45(22), 12639–12646. <https://doi.org/10.1029/2018GL079802>.
- Baldwin, M.P., Ayarzagüena, B., Birner, T., Butchart, N. and Pedatella, N.M. (2020) Sudden Stratospheric Warmings. *Earth and Space Science Open Archive*. preprint. Earth and Space Science Open Archive.
- Baldwin, M.P. and Dunkerton, T.J. (2001) Stratospheric harbingers of anomalous weather regimes. *Science (New York, N.Y.)*. American Association for the Advancement of Science, 294(5542), 581–584. <https://doi.org/10.1126/science.1063315>.
- Beerli, R. and Grams, C.M. (2019) Stratospheric modulation of the large-scale circulation in the Atlantic–European region and its implications for surface weather events. *Quarterly Journal of the Royal Meteorological Society*. John Wiley and Sons Ltd, 145(725), 3732–3750. <https://doi.org/10.1002/qj.3653>.
- Bevacqua, E., Shepherd, T.G., Watson, P.A.G., Sparrow, S. and Mitchell, D. (2021) Larger spatial footprint of wintertime total precipitation extremes in a warmer climate. *Geophysical Research Letters*, 48(8). <https://doi.org/10.1029/2020GL091990>.
- Byrne, N.J., Shepherd, T.G. and Polichtchouk, I. (2019) Subseasonal-to-seasonal predictability of the Southern Hemisphere eddy-driven jet during austral spring and early summer. *Journal of Geophysical Research: Atmospheres*. Blackwell Publishing Ltd, 124(13), 2018JD030173. <https://doi.org/10.1029/2018JD030173>.
- Charlton, A.J. and Polvani, L.M. (2007) A new look at stratospheric sudden warmings. Part I: climatology and modeling benchmarks. *Journal of Climate*, 20(3), 449–469. <https://doi.org/10.1175/JCLI3996.1>.
- Domeisen, D.I.V. and Butler, A.H. (2020) Stratospheric drivers of extreme events at the Earth's surface. *Communications Earth & Environment*. Springer Science and Business Media LLC, 1(1), 1–8. <https://doi.org/10.1038/s43247-020-00060-z>.
- Domeisen, D.I.V., Grams, C.M. and Papritz, L. (2020) The role of North Atlantic–European weather regimes in the surface impact of sudden stratospheric warming events. *Weather and Climate Dynamics*. Copernicus GmbH, 1(2), 373–388. <https://doi.org/10.5194/wcd-1-373-2020>.
- Hersbach, H., Bell, B., Berrisford, P., Hirahara, S. and Thépaut, J. (2020) The ERA5 global reanalysis. *Quarterly Journal of the Royal Meteorological Society*, 146, qj.3803. <https://doi.org/10.1002/qj.3803>.
- Hitchcock, P., Shepherd, T.G. and Manney, G.L. (2013) Statistical characterization of Arctic polar-night jet oscillation events. *Journal of Climate*. American Meteorological Society, 26(6), 2096–2116. <https://doi.org/10.1175/JCLI-D-12-00202.1>.
- Hitchcock, P. and Simpson, I.R. (2014) The downward influence of stratospheric sudden warmings. *Journal of the Atmospheric Sciences*, 71(10), 3856–3876. <https://doi.org/10.1175/JAS-D-14-0012.1>.
- Jiménez-Esteve, B. and Domeisen, D.I.V. (2018) The tropospheric pathway of the ENSO–North Atlantic teleconnection. *Journal of Climate*, 31(11), 4563–4584. <https://doi.org/10.1175/JCLI-D-17-0716.1>.
- Johnson, S.J., Stockdale, T.N., Ferranti, L., Balmaseda, M.A. and Monge-Sanz, B.M. (2019) SEAS5: the new ECMWF seasonal forecast system. *Geoscientific Model Development*. Copernicus GmbH, 12(3), 1087–1117. <https://doi.org/10.5194/gmd-12-1087-2019>.

- Karpechko, A.Y. and Manzini, E. (2012) Stratospheric influence on tropospheric climate change in the Northern Hemisphere. *Journal of Geophysical Research: Atmospheres*, 117(D5). <https://doi.org/10.1029/2011JD017036>.
- Karpechko, A.Y., Hitchcock, P., Peters, D.H.W. and Schneidereit, A. (2017) Predictability of downward propagation of major sudden stratospheric warmings. *Quarterly Journal of the Royal Meteorological Society*. John Wiley & Sons, Ltd. 143 (704), 1459–1470. <https://doi.org/10.1002/qj.3017>.
- Kautz, L., Polichtchouk, I., Birner, T., Garny, H. and Pinto, J.G. (2020) Enhanced extended-range predictability of the 2018 late-winter Eurasian cold spell due to the stratosphere. *Quarterly Journal of the Royal Meteorological Society*. John Wiley and Sons Ltd, 146(727), 1040–1055. <https://doi.org/10.1002/qj.3724>.
- Kidston, J., Scaife, A.A., Hardiman, S.C., Mitchell, D.M. and Gray, L.J. (2015) Stratospheric influence on tropospheric jet streams, storm tracks and surface weather. *Nature Geoscience*, 8(6), 433–440. <https://doi.org/10.1038/ngeo2424>.
- King, A.D., Butler, A.H., Jucker, M., Earl, N.O. and Rudeva, I. (2019) Observed relationships between sudden stratospheric warmings and European climate extremes. *Journal of Geophysical Research: Atmospheres*. Blackwell Publishing Ltd, 124(24), 13943–13961. <https://doi.org/10.1029/2019JD030480>.
- King, M.P., Li, C. and Sobolowski, S. (2021) Resampling of ENSO teleconnections: accounting for cold season evolution reduces uncertainty in the North Atlantic. *Weather and Climate Dynamics Discussions*. Copernicus GmbH, 2, 759–776. <https://doi.org/10.5194/wcd-2-759-2021>.
- Kodera, K., Mukougawa, H., Maury, P., Ueda, M. and Claud, C. (2016) Absorbing and reflecting sudden stratospheric warming events and their relationship with tropospheric circulation. *Journal of Geophysical Research: Atmospheres*, 121(1), 80–94. <https://doi.org/10.1002/2015JD023359>.
- Kretschmer, M., Adams, S.V., Arribas, A., Prudden, R. and Shepherd, T.G. (2021) Quantifying causal pathways of teleconnections. *Bulletin of the American Meteorological Society*. American Meteorological Society, 1(aop), 1–34. <https://doi.org/10.1175/BAMS-D-20-0117.1>.
- Kretschmer, M., Cohen, J., Matthias, V., Runge, J. and Coumou, D. (2018a) The different stratospheric influence on cold-extremes in Eurasia and North America. *npj Climate and Atmospheric Science*. Nature Publishing Group, 1(1), 44. <https://doi.org/10.1038/s41612-018-0054-4>.
- Kretschmer, M., Coumou, D., Agel, L., Barlow, M. and Cohen, J. (2018b) More-persistent weak stratospheric polar vortex states linked to cold extremes. *Bulletin of the American Meteorological Society*, 99(1), 49–60. <https://doi.org/10.1175/BAMS-D-16-0259.1>.
- Matthias, V. and Kretschmer, M. (2020) The influence of stratospheric wave reflection on north American cold spells. *Monthly Weather Review*. American Meteorological Society, 148(4), 1675–1690. <https://doi.org/10.1175/MWR-D-19-0339.1>.
- Maycock, A.C. and Hitchcock, P. (2015) Do split and displacement sudden stratospheric warmings have different annular mode signatures? *Geophysical Research Letters*, 42(24), 10943–10951. <https://doi.org/10.1002/2015GL066754>.
- McLandress, C. and Shepherd, T.G. (2009) Impact of climate change on stratospheric sudden warmings as simulated by the Canadian middle atmosphere model. *Journal of Climate*. American Meteorological Society, 22(20), 5449–5463. <https://doi.org/10.1175/2009JCLI3069.1>.
- Polichtchouk, I., Shepherd, T.G. and Byrne, N.J. (2018a) Impact of parametrized nonorographic gravity wave drag on stratosphere-troposphere coupling in the Northern and Southern Hemispheres. *Geophysical Research Letters*, 45(16), 8612–8618. <https://doi.org/10.1029/2018GL078981>.
- Polichtchouk, I., Shepherd, T.G., Hogan, R.J. and Bechtold, P. (2018b) Sensitivity of the Brewer–Dobson circulation and polar vortex variability to parameterized nonorographic gravity wave drag in a high-resolution atmospheric model. *Journal of the Atmospheric Sciences*. American Meteorological Society, 75(5), 1525–1543. <https://doi.org/10.1175/JAS-D-17-0304.1>.
- Runde, T., Dameris, M., Garny, H. and Kinnison, D.E. (2016) Classification of stratospheric extreme events according to their downward propagation to the troposphere: CLASSIFICATION OF STRATOSPHERIC EVENTS. *Geophysical Research Letters*, 43(12), 6665–6672. <https://doi.org/10.1002/2016GL069569>.
- Scaife, A.A., Spangehl, T., Fereday, D.R., Cubasch, U. and Shepherd, T.G. (2012) Climate change projections and stratosphere–troposphere interaction. *Climate Dynamics*, 38(9–10), 2089–2097. <https://doi.org/10.1007/s00382-011-1080-7>.
- Stockdale, T., Johnson, S., Ferranti, L., Balamseda, M. and Briceag, S. (2018) ECMWF's new long-range forecasting system SEAS5. *ECMWF Newsletter*, 154, 15–20. <https://www.ecmwf.int/node/18202>.
- Tietsche, S., Balamseda, M., Zuo, H., Roberts, C. and Ferranti, L. (2020) The importance of North Atlantic Ocean transports for seasonal forecasts. *Climate Dynamics*, 55(7), 1995–2011. <https://doi.org/10.1007/s00382-020-05364-6>.
- Vitart, F. and Robertson, A.W. (2018) The sub-seasonal to seasonal prediction project (S2S) and the prediction of extreme events. *npj Climate and Atmospheric Science*. Springer US, 1(1), 1–7. <https://doi.org/10.1038/s41612-018-0013-0>.
- Waugh, D.W., Sobel, A.H. and Polvani, L.M. (2017) What is the polar vortex, and how does it influence weather? *Bulletin of the American Meteorological Society*, BAMS-D-15-00212.1. 98(1), 37–44. <https://doi.org/10.1175/BAMS-D-15-00212.1>.
- White, I., Garfinkel, C.I., Gerber, E.P., Jucker, M. and Oman, L.D. (2019) The downward influence of sudden stratospheric warmings: association with tropospheric precursors. *Journal of Climate*. American Meteorological Society, 32(1), 85–108. <https://doi.org/10.1175/JCLI-D-18-0053.1>.
- Zappa, G., Hoskins, B.J. and Shepherd, T.G. (2015) The dependence of wintertime Mediterranean precipitation on the atmospheric circulation response to climate change. *Environmental Research Letters*. IOP Publishing, 10(10), 104012. <https://doi.org/10.1088/1748-9326/10/10/104012>.
- Zappa, G. and Shepherd, T.G. (2017) Storylines of atmospheric circulation change for European regional climate impact assessment. *Journal of Climate*. American Meteorological Society, 30(16), 6561–6577. <https://doi.org/10.1175/JCLI-D-16-0807.1>.

**How to cite this article:** Monnin, E., Kretschmer, M., & Polichtchouk, I. (2021). The role of the timing of sudden stratospheric warmings for precipitation and temperature anomalies in Europe. *International Journal of Climatology*, 1–15. <https://doi.org/10.1002/joc.7426>